Influence of the Shape Memory Alloys on Endplate Connections and Residual Deformation

Amin Komeily[1], Mohammad Reza Shokoohfar[2], Mehdi Ghassemieh[3], Mohammad Shakerian[4]

[1] School of Civil Engineering, College of Engineering, University of Tehran; amin.komeili.98@ut.ac.ir

[2] School of Civil Engineering, College of Engineering, University of Tehran; mreza.shokoohfar@ut.ac.ir

[3] School of Civil Engineering, College of Engineering, University of Tehran; m.ghassemieh@ut.ac.ir

[4] School of Civil Engineering, College of Engineering, University of Tehran; mshakerian@ut.ac.ir

Abstract

Yielding in steel structures dissipates seismic energy, which results in residual deformations. Conventional lateral-resisting systems provide appropriate seismic safety. However, these systems undergo severe structural damage when exposed to strong ground motions. Seismic residual drifts make it difficult or impossible to fix damaged structures. Therefore, systems that can reduce seismic residual deformations are required. Superelastic shape memory alloys (SMAs) can withstand significant deformations and recover all plastic deformations upon unloading. They can significantly lessen seismic residual deformations in steel structures, making post-seismic retrofitting easier. This paper will compare the use of a superelastic Ni-Ti alloy and a Fe-based SMA in two endplate connections of NIST benchmark buildings (NIST Technical Note 1863-3). In addition, some features that lead to decreased residual deformation in these types of joints will be investigated.

Keywords (Times New Roman bold 11 pt.): Shape memory alloys, Superelastisity, Finite element method, self-centering, Endplate connection, Residual deformation.

Introduction

Until the 1990s, Steel moment resisting frames with fully restrained welded beam-to-column connections (such as joints with welded beam flange) had long been accepted as a suitable structural solution against seismic loadings. The 1994 Northridge and 1995 Kobe earthquakes revealed the deficiencies in these connections. Such connections, which at the time represented the majority of connections, frequently failed due to weld fracture. Later, a study known as the SAC Project was started to look at the causes of the extensive weld fracture and, as a result, make recommendations for better connection specifications for steel structures against earthquakes (FEMA 2000). This project provided significant insight into the use of bolted steel connections in seismic applications [1, 2], and it was found that when properly designed and detailed, bolted connections would provide high seismic performance with adequate strength, ductility, and stiffness for seismic performance. Relevant test results demonstrated that a "strong-connection-weak-beam" theory was the preferred design method, allowing plastic hinges to be developed over the beam portion close to the connection region [3-5].

Additionally, it was discovered that more flexible semi-rigid connections could be used as a substitute to provide adequate plastic rotations and reliable seismic performances [1]. The typical design approaches for seismic resistant connections generally result in post-earthquake deformations in the beams (strong connections) or in the connections (partial strength connections), which are expensive and problematic to repair. Researchers are developing novel design strategies to reduce seismic residual deformations. For instance, to provide a recentering mechanism after an earthquake, special post-tensioned bars were installed in connections [6, 7].

Shape memory alloys (SMAs) have also received much attention due to their self-centering and damping characteristics, and connections with shape memory alloys (SMAs) have lately appeared as a promising substitute for reaching the self-centering purpose [8]. The SMAs made of nickel-titanium (Ni-Ti) received the most extensive research [9].

Shape Memory Effect (SME) and superelasticity (SE) are the two main characteristics of SMAs. SME refers to a material's potential to recover from significant mechanically produced strains by gradually raising its temperature. SE refers to a material's capacity to sustain large inelastic strains and recover its initial shape after load removal. Furthermore, the base isolations and dampers used as passive control devices, which have concerns with aging, durability, and maintenance, may no longer be necessary due to SMA's high corrosion resistance performance (equal to stainless steel).

An external beam-column connection using martensite SMA rods was put to the test by Ocel et al. [10]. The connection demonstrated excellent energy dissipation, significant ductility, and no strength degradation up to a 4% drift level. Besides, When the SMA tendons were heated, the connection recovered 76% of the previous drift. DesRoches et al. [11] investigated SMA bars and wires, particularly SMAs with large cross-sections, to determine cyclic properties and their potential for seismic design and retrofit purposes. In this study, the effects of bar size, loading frequency, and yield stress on damping, recentering, and recentering capability was conducted to assess their feasibility for utilization in seismic applications. DesRoches et al. [12] and Ellingwood et al. [13] used SMA bars in novel beam-to-column connections to evaluate the seismic performance of SMRFs incorporating these connections. The recentering characteristic and high energy dissipation were produced using superelastic SMA connections and martensite SMA connections, respectively. Nonlinear time history studies were conducted to determine how these connections affected peak and residual inter-story drifts. An extended endplate connection using SMA bolts was suggested by Ma et al. [14]. The superelastic SMA bolts were used for this type of connection instead of the conventional high strength (HS) bolts. The deformation of SMA bolts accomplished the energy dissipation and ductility requirements. Thus, the superelastic hinge could develop inside the connection while the adjacent structural members (endplate, beam, and column) are mostly within the elastic range. This design approach's innovative benefit is reducing the need for structural member repairs after an earthquake, which will significantly lower the cost of retrofit work. An experimental quasi-static analysis was performed by Ma and Yam [15] to look into the seismic performance of endplate connections that were equipped with eight long SMA bolts. Nearly all of the drift was recovered by unloading, plastic deformation was restricted to SMA bolts with relatively large capacities, and all beams and columns stayed within the elastic range. Speicher et al. [16] experimentally evaluated four beams to column connections incorporating superelastic Ni-Ti tendons, martensite Ni-Ti tendons, and a combination of Ni-Ti and Aluminum tendons under cyclic loading. After a maximum drift of 5%, both Ni-Ti tendons demonstrated a significant level of self-centering, with residual deformations measured between 0.5 and 1%. Extended endplate connections with superelastic bolts in an MRF were analyzed experimentally and numerically by Fang et al. [17, 18]. SMA connections exhibited high recentering ability and proper energy dissipation. Slender (long with a small diameter) SMA bolts represented more ductile connections.

Farmani and Ghassemieh [19] numerically studied two innovative types of beam-column connections. Including SMA tendons and shear-resisting elements like shear tabs and web hourglass steel pins into the connection improved the connection's energy dissipation, moment capacity, and shear resistance. However, if these components had been improperly designed, they would have compromised the connection's self-centering, stiffness, and energy dissipation. Sultana and Youssef [20] investigated where the SMA connections should be installed in various MRFs to minimize residual drifts after a seismic event while considering the maximum inter-story drift during an earthquake. Roshanfekr Rad et al. [21] probabilistically studied the seismic performance of two typical lateral load-resisting systems, including MRF and EBF, which incorporated superelastic SMA bolts in their beam-column connections and link-beam connections, respectively. Effects of SMA connections on peak inter-story drifts and residual drifts were investigated. Also, comparisons between conventional and SMA connections in terms of life safety performance and repair cost were performed.

Although employing Ni-Ti SMAs to achieve structural self-centering after earthquakes has enormous potential, SMA components are expensive. A significant effort has been made to produce other SMAs, such as iron-based SMAs, which are appropriate for use in large-scale civil engineering applications (Cladera et al. [22]). Tanaka et al. [23] presented an iron-based polycrystalline SMA (an alloy made of Fe-Ni-Co-Al-Ta-B) that showed extremely high tensile strength (more than 1000 MPa) and a superelastic strain above 13% at room temperature. In addition, Omori et al. [24] discovered another iron-based SMA (Fe-Mn-Al-Ni), with a recoverable strain of more than 5%, showed acceptable superelastic characteristics at room temperature. Nazari and Ghiami Azad et al. [25] numerically studied endplate connections equipped with Fe-based SMA introduced by Omori et al. [24]. These connections' moment capacity, stiffness, recentering ability, and energy dissipation were compared with conventional endplate connections.

Numerical Model Verification

The Abaqus finite element software was used to create and analyze 3D models to evaluate the response of extended endplate connections equipped with SMA bolts. Before beginning the in-depth analysis, it is required to first validate the SMA connection model. For this purpose, one of the experimentally tested endplate connections is equipped with SMA bolts (Fang et al. [26]) is chosen to make a comparison between finite element model and test results. The fourth specimen ("SMA-D10-290") is an edge beam-column connection in which a cantilever beam connected to a column by an extended endplate welded to the beam end and HS bolts are substituted by long superelastic SMA bolts. The beam dimensions for the SMA connection specimens were chosen to guarantee that the beams would stay elastic while applying the cyclic load. Geometric details and mechanical properties of steel materials used in the experimental specimen are depicted in “Figure 1” and “Table 1”, respectively.

Table 1. Material properties of steel

Material	Modulus of Elasticity (GPa)	Yield Strength (MPa)	Ultimate Strength (MPa)	Fracture Strain (%)
Steel (beam)	210.1	287.5	452.9	28.3
Steel (end-plate)	205.6	377.5	531.2	24.9
Steel (column)	193.3	306.1	487.4	26

Bilinear stress-strain relationships were considered for steel materials, and the elastic modulus and Poisson ratio were assumed to be 200 GPa and 0.3, respectively. Additionally, combined (isotropic-kinematic) hardening was chosen in the numerical model for steel material's plasticity and nonlinearity.

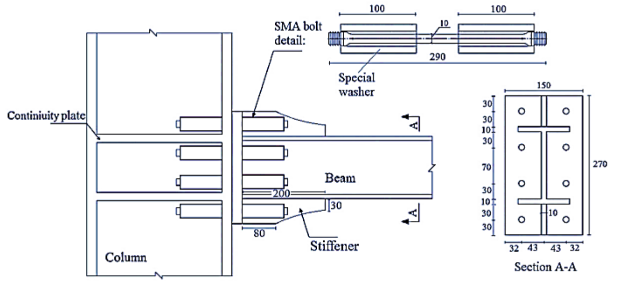

Figure 1.Description of experimental model [26]

Auricchio's model (Auricchio et al. [27]) was used to define the superelastic behavior of SMA in the Abaqus software. In Auricchio's model, the key parameters utilized to characterize a superelastic SMA material are the elastic moduli of SMA in the austenite and martensite phases (EA, EM), transformation stresses (σMs, σMf, σAs, and σAf), maximum transformation strain (εl), and Poisson ratios (νA, νM). This model indicates that the external force-induced deformations in the SMA material can be entirely recovered after unloading under isothermal circumstances. Furthermore, residual cumulative strains under cyclic loads are omitted, and there is no connection between loading rate and material behavior.

In the experimental study, The Ni-Ti bars, similar in type and diameter to the SMA bolts in the tested connections, were subjected to coupon tests at room temperature [28]. Based on these results, the SMA nominal properties are mentioned in the “Table 2”. In the numerical model, these engineering values are converted to actual stress-strain values.

Table 2. Material properties of SMA bolt used in Abaqus ([26])

Material properties	Value
Modulus of elasticity E_A (GPa)	40
Modulus of elasticity E_M (GPa)	40
Austenite-to-martensite starting stress σ^{Ms} (MPa)	350
Austenite-to-martensite finishing stress σ^{Mf} (MPa)	450
Martensite-to-austenite finishing stress σ^{As} (MPa)	150
Martensite-to-austenite finishing stress σ^{Af} (MPa)	75
Poisson ratios ν_A, ν_M	0.33
Transformation strain ε_L (%)	5

All components were built using solid parts. Large displacements and strains were more precisely considered using nonlinear geometry (an option in Abaqus) throughout loading steps. As mentioned before, corresponding to design details, which beams stayed in the elastic range, buckling did not happen, and regarding [29] half modeling of connections considering symmetric boundary conditions can be used without inaccuracy. This method leads to faster computation time without affecting the outcomes. The symmetry plane passes through beam and column center lines.

For all contacts, hard contact with a friction coefficient of 0.2 was used, which is equivalent to the Class D slip coefficient (Eurocode 3 [30]). since the weld material is stronger than structural steel, The welded parts were incorporated utilizing surface-based "Tie" constraints.

Apart from symmetry, other boundary conditions are identical to those in the experimental model. The transitional degrees of freedom were constrained by defining boundary conditions on the column top and bottom surfaces (fixed support condition). Three-dimensional, eight-node linear brick elements with reduced integration were used to mesh each part of the model (C3D8R). SMA bolts were meshed with the same elements but with a nonreduced integration method.

Typically, loading consists of two steps. The first step included pre-strain which would result in prestresses, and the second step referred to mechanical load (i.e., beam tip drift). By applying a negative temperature gradient to the bolts' shanks, pre-tensioning was accomplished. For SMA material, the thermal expansion coefficient needs to be high in order to prevent errors caused by large temperature gradients. Additionally, orthotropic expansion was defined to provide thermal contraction in a single direction (bolt longitudinal axis). The temperature variation was selected so that all the SMA bolts would experience approximately 230 MPa prestress, about 65% of forward transformation stress. This preload was applied for initial stiffness, self-centering ability, and sufficient friction between the endplate and column face [31]. further levels of pretension would result in bolt twisting [26]. Speicher et al. [30], in another experimental study on the SMA-equipped connections, revealed that pre-strain more than 0.5% would be impractical due to the tendency of bolt shanks to twist.

The second step included vertical displacement of the beam tip under the SAC loading protocol [2, 30]. This protocol stipulates several load cycles with increasing inter-story drift levels. The inter-story drift should be calculated by dividing the beam tip displacement by the distance between the column center and the loading point. It is noteworthy to mention that in the finite element analysis, only one load cycle was conducted for each drift level to increase the computation rate. Some instructions are necessary for finite element analysis to prevent numerical problems. Mesh quality should be evaluated to identify distorting elements (if there are any), slave surfaces mesh density should be finer than master surfaces mesh density, each drift level should be applied in several increments according to nonlinearity, etc.

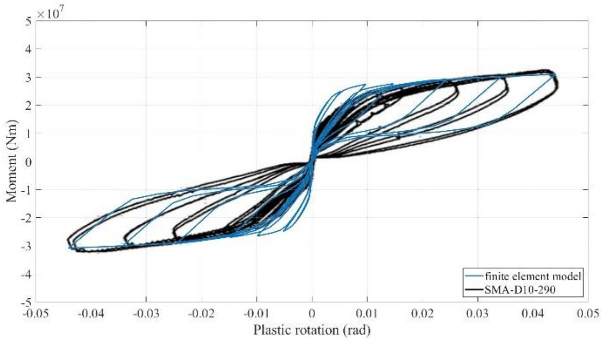

Figure 2. Verification of the numerical analysis

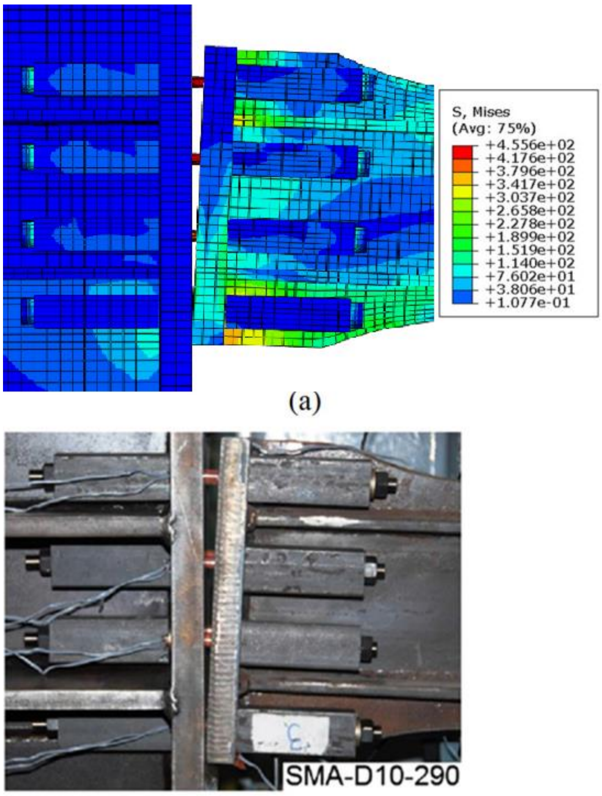

Figure 3. (a) Deformed shape and von Mises stress contour of the numerical model at 5% drift in comparison with (b) the deformed shape of the experimental specimen [26]

"Figure 2" shows the relationship between the connection plastic rotation for analytical and experimental models and the bending moment at the column face. The plastic rotation was calculated by subtracting the beam's elastic rotation from the overall drift. The elastic rotation of the beam is equal to the applied force divided by elastic stiffness derived from a model with rigid bolts (Fang et al. [26]).

Because of the limitation of the SMA material constitutive model, the hysteresis curve generated by the numerical model does not perfectly match the experiment's outcomes. The differences between the unloading regions of the two curves are primarily due to SMA model idealizations. However, the numerical model accurately predicted the test specimen's overall cyclic response concerning stiffness, strength, energy dissipation, and self-centering ability.

"Figure 3" depicts the connection's deformed shape at the ultimate drift level. As shown, the finite element model deformation and the deformation of the experimental specimen closely match.

Connection's General Design Procedure

Two beam-column connections were selected from NIST benchmarks in order to compare the cyclic response of extended endplate connections equipped with a tested Ni-Ti and an iron-based SMA. Aside from the SMA bolts, AISC design guides were used to design the other parts of the connections. For diminishing prying actions, thick endplates are chosen in designs. Steel material was A992 (F_y= 50 ksi, F_u= 65 ksi) and SMAs' properties are listed in "Table 3".

Table 3. Material properties of SMAs used in this study

Material	Ni-Ti [31]	Fe-Mn-Al-Ni [24]
E_A (ksi)	4350	14200
E_M (ksi)	2900	8690
σ_{Ms} (ksi)	44	46
σ_{Mf} (ksi)	65	58
σ_{As} (ksi)	29	30
σ_{Af} (ksi)	15	13
ν_A, ν_M	0.33	0.33
ε_L (%)	5	5

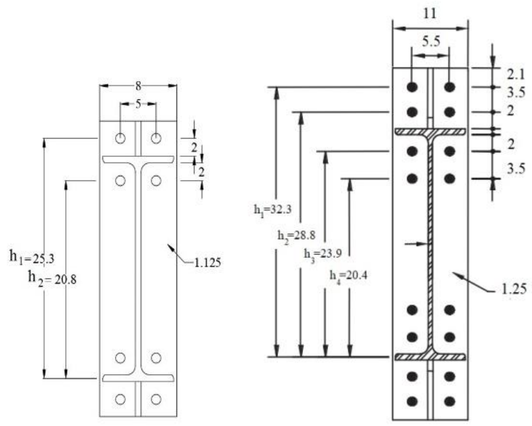

Figure 9. connections' geometry

Each model's name identification is divided into three parts: connection type, SMA type, and bolt length, respectively. The first part stands for connection type:

- EC4 4-bolt
- EC4S 4-bolt with endplate stiffeners
- EC8S 8-bolt with endplate stiffeners

The second part represents the SMA type:

- Ni for Ni-Ti and Fe for Fe-based SMAs.

The third part introduces SMA bolts length:

- L for long bolts (12.5 inches)
- I for intermediate bolts (10 inches)
- S for short bolts (7.5 inches).

These lengths are approximately equal to 50%,40%, and 30% of the beam's depth. There are two connections in which the SMA bolts are one grade smaller (in diameter), in which the letter W follows their names. For instance, the name EC4-Fe-I represents a 4-bolt extended endplate connection utilizing Fe-based SMAs in which the shanks are 10 inches.

Table 4. beams, columns, and SMA diameters

connection	beam	column	bolts' diameters (inch)
4-bolted	W24X55	W14X145	1.125 (1 for weaker)
8-bolted	W27X114	W18X175	1.25 (1.125 for weaker)

SMA Bolts Design Procedure

In conventional procedures, plastic hinges develop on the beam ends as the structure experiences seismic excitations. On the other hand, in SMA-equipped connections, the plastic or, more precisely, the superelastic hinge is located at the beam-column interface, where SMA bolt elongation results in a ductile connection. This purpose can be accomplished by choosing lower values for the bolt series' moment capacity relative to the beam flexural resistance.

Sultana and Youssef [20] in their study on moment-resisting frames equipped with SMA connections, assumed that:

$$0.8M_{pb} = 2\,\sigma_{ms} \times \pi d_b^2/4 \times (\sum h_i)$$

M_{pb} is the beam plastic bending moment, d_b is bolts diameter, σ_{ms} is forward transformation stress of SMA material, and $h_i$is depicted in "figure 9". In another study conducted by Roshanfekr Rad et al. [21], the diameter of the bolts was chosen differently:

$$M_{y,beam} = (\sigma_{ms} + \sigma_{mf}) \times \pi d_b^2/4 \times (\sum h_i)$$

Where $M_{y,beam}$ is the elastic moment capacity of the beam section and σ_{mf} is the final stress for forward phase transformation of SMA.

This study used the second approach to calculate the Ni-Ti bolts' diameters. Fe-based SMAs with the same diameter as Nitinol bolts were incorporated into the connections to compare Ni-Ti with Fe-based SMA bolts. Bolts diameters are listed in the "Table 3".

All the SMA bolts received a pre-strain of 0.5% at the bolt pre-tensioning stage. SMA shanks were subjected to a negative temperature gradient to make the average longitudinal stress in the center of the bolts equal to $\frac{0.5}{100} E_A$ (stress at 0.5% strain).

The loading process was carried out similar to the SAC loading protocol [31] with two additional drift levels (5% and 6%). It should be noted that as a verification model, every drift level was applied for one cycle to reduce computational time. The properties of SMA materials are listed in "Table 3".

Results and Discussions

This section presents the cyclic behavior of the six connection models. "Figure 4" illustrates the deformed shape of three models at 6% drift level. Due to limitation of SMA bolts in these types of connections, designing a connection which deforms without beam yielding at high drift levels isn't practicable. therefore, plastic strains are remained in parts of the beams.

"Figures 4-8" illustrate end-plate connections' moment-rotation hysteresis. The sections below discuss about connections' recentering, strength, stiffness and energy dissipation.

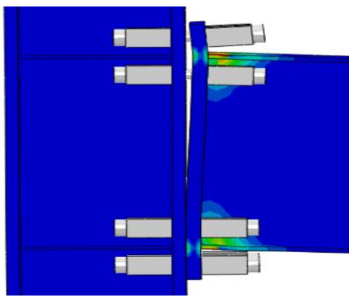

(a)

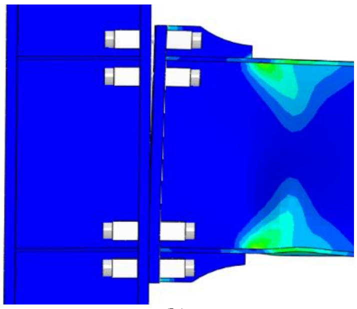

(b)

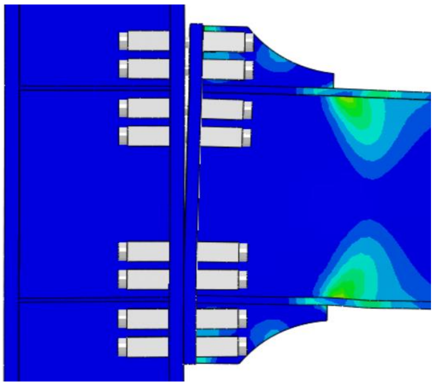

(c)

Figure 4. deformed shape of connections at final drift level. (a) EC4-Fe-I, (b) EC4S-Ni-S, and (c) EC8S-Fe-L

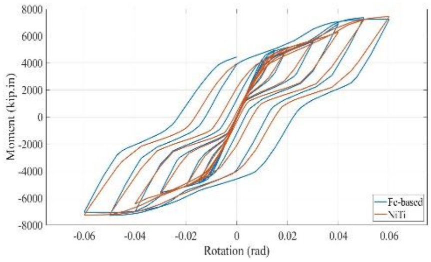

(a) EC4S-Fe & Ni-I

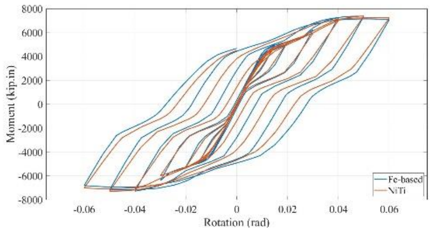

(b) EC4S-Fe & Ni-S

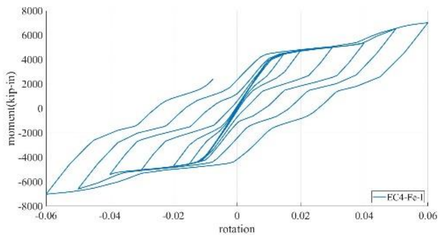

(c) EC4-Fe-I

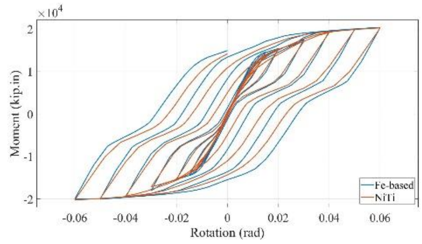

(d) EC8S-Fe & Ni-I

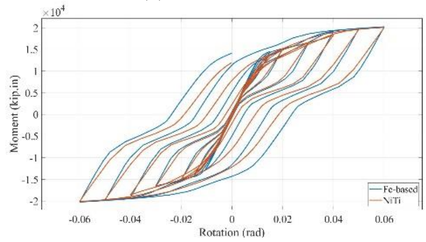

(e) EC8S-Fe & Ni-L

Figure 5. moment-interstory drift of connections

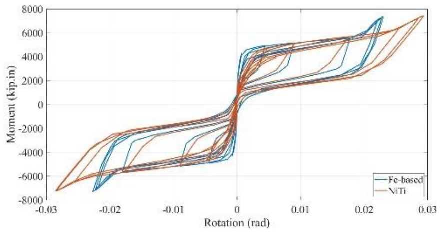

(a) EC4S-Fe & Ni-I

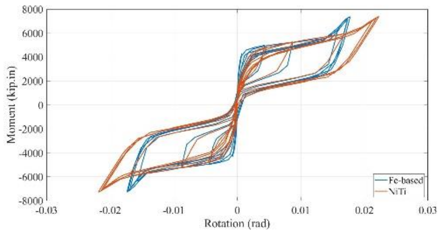

(b) EC4S-Fe & Ni-S

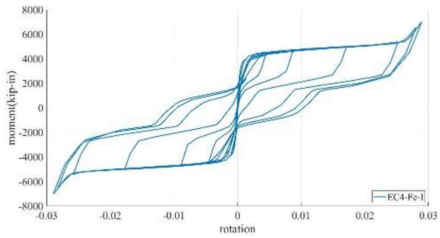

(c) EC4-Fe-I

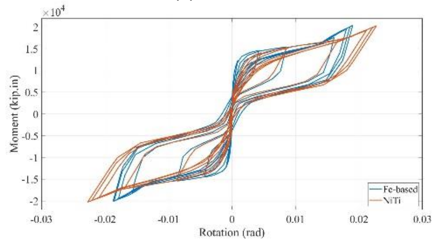

(d) EC8S-Fe & Ni-I

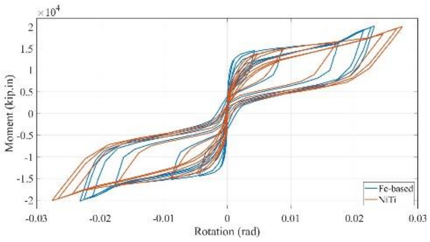

(e) EC8S-Fe & Ni-L
Figure 6. moment-rotation joints

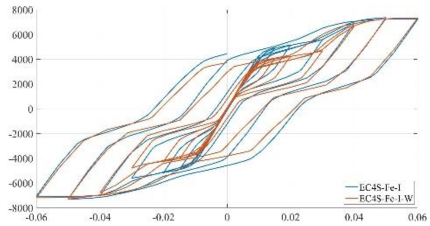

Figure 7. moment inter-story drifts, EC4S-Fe-I & EC4S-Fe-I-W

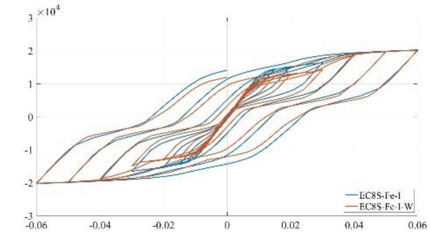

Figure 8. moment-inter-story drifts, EC8S-Fe-L & EC8S-Fe-L-W

recentering

An evaluation of the residual drifts can be used to estimate a beam-column connection's self-centering capacity. Following is a definition of the self-centering index (SCI) of the connections at each inter-story drift level:

$$SCI_\theta = 100\,(1 - \frac{\theta_r}{\theta})$$

Where SCI_θ is the percentage of the connection recentering (self-centering) ability after an inter-story drift level of θ and θ_r is the residual drift. “Figures 9 a and b” depict the SCI_θ for 4-bolted and 8-bolted end-plate connections, respectively. At drifts of 0.02 rad and below, the recentering indices for all connections were more than 96%, meaning that the connections were able to totally restore their initial states after unloading.

Although thick end-plate was chosen for EC4-Fe-I, the recentering capacity of this connection isn't satisfactory. by stiffening end-plate the SCI_θ for EC4S-Fe-I significantly improved.

as drift levels go further, the recentering ability of connections diminishes due to two main reasons. the first reason is that as joint exposed to higher levels of rotation, yielding in end-plates stiffeners, which is produced by concentrated compressive forces, increases. also, high level of drifts results in end-plate flexural yielding around farthest bolt rows. the second reason is that when SMA bolts' stresses goes beyond the σmf, beam reaches it is plastic moment capacity and plastic hinge develops on the beam end.

Models with weaker SMAs didn't exhibit a considerable difference in SCI_θ due to joint plastic deformation (i.e., the second reason mentioned above).

Overall, intermediate and long bolt lengths for 4-bolted and 8-bolted connections seems to be more efficient to reduce residual drifts, respectively. Furthermore, almost all the connections equipped with iron-based SMAs, demonstrated good recentering which weren't far from Ni-Ti connections.

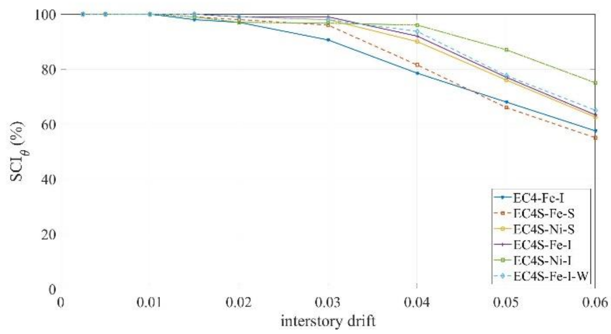

(a)

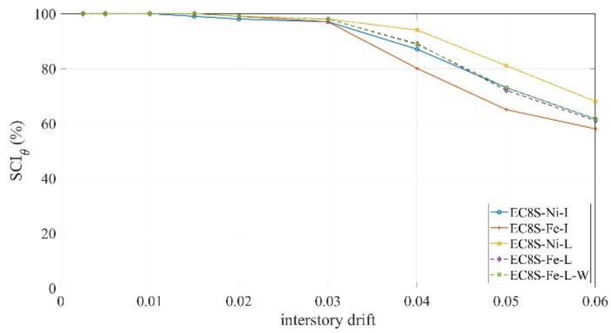

(b)

Figure 9. SCI_θ (a) 4-bolted and (b) 8-bolted

strength and stiffness

All the connections reached the plastic moment capacity of connected beams at 6% drift. So, all of them are full-strength connections.

“Table 4” shows the stiffness of the connections. Longer bolts made connections less stiff, without changing the final moment capacity. if a connection's initial stiffness (Kcon) for moment-resisting frames is greater than 25EI/L (where EI/L is the stiffness of the connected beam and is twice the length of cantilever beam), the connection is in rigid category. on the other hand, when K_{con} is less than 0.5EI/L, the connection is regarded to be nominally pinned, and connections with initial stiffness between the two limits are considered semi-rigid. Therefore, according to numerical results, these connections are characterized as semi-rigid connections.

Table 4. connections' rotational stiffness

CONNECTION	K_{con} (*10^6 kip.in/rad)	K_{con}/(EI/L)
EC4-Fe-I	1.9	17.5
EC4S-Fe-I	2.3	21.2
EC4S-Ni-I	1	9.2
EC4S-Fe-S	2.4	22.2
EC4S-Ni-S	1.54	14.2
EC4S-Fe-I-W	1.9	17.5
EC8S-Fe-I	6.6	20.1
EC8S-Ni-I	3.7	11.3
EC8S-Fe-L	6.4	19.5
EC8S-Ni-L	3.46	10.5
EC8S-Fe-L-W	6.15	18.7

Table 5. dissipated energy

dissipated energy (kip.in)		
CONNECTION	total	joint
EC4-Fe-I	1222	710
EC4S-Fe-I	1394	534
EC4S-Ni-I	1041	522
EC4S-Fe-S	1670	444
EC4S-Ni-S	1370	446
EC4S-Fe-I-W	1197	570
EC8S-Fe-I	4952	1437
EC8S-Ni-I	4064	1341
EC8S-Fe-L	4275	1628
EC8S-Ni-L	3329	1461
EC8S-Fe-L-W	4162	1915

energy absorption

The cumulative energy dissipation (the area encompassed by the hysteresis loops) was determined for both joints and total rotations to gain a better understanding of the cyclic performance of the models. “Table 5” illustrates dissipated energy in all models. As expected, joints with shorter bolts showed lower damping. However, overall damping of these models were more than the others with longer SMA bolts. In other words, Beams' plastic hinges increased overall dissipated energy.

EC4-Fe-I dissipated more energy in it's joint in relation to EC4S-Fe-I. this was happened because of plastic deformations occurred in the unstiffened end-plate. Total energy absorption in the second connection was about 14% more than the first one which indicates higher plasticity in the stiffened connection's beam.

In all cases, iron-based SMA joints exhibited approximately similar levels of energy dissipation. However, overall energy absorption in Ni-Ti connections was lower numbers. That is induced by significantly higher stiffness of Fe-based SMA bolts. In addition, models incorporating weaker bolts can be used with respect to their capacity to act as full-strength connections (which results in decrease of SMA material usage). In fact, the final moment capacity of connections for weaker models as others is dependent to beams' plastic moment.

Conclusion

in this article, the cyclic response of two different beam-to-column connections were numerically investigated to compare the performance of end-plate connections equipped with two different types of superelastic SMA bolts. following conclusions were extracted from the finite element results:

- First, comparisons with the test data were used to validate the FE modelling method. It was shown that the test results and the FE results had acceptable agreement.
- since in SMA equipped connections, the ductility and recentering capability are mostly provided by elongation of SMA bolts, incorporating longer SMAs would result in higher superelastic ductility and recentering.
- Hysteretic curves showed that using SMAs with one grade smaller diameters didn't change the maximum moment capacity of the connections at high drift levels. However, before drifts of about 4%, the resistance of models was significantly depended on SMAs' diameters.
- Iron-based SMA can be a substitute for Ni-Ti. Results showed that the recentering ability of connections equipped with Fe-based SMA bolts, can accommodate self-centering almost equal to connections used Ni-Ti bolts. Also due to higher module of elasticity in iron-based SMAs, connections utilized iron-based bolts had higher levels of stiffness.
- Due to high cost of Ni-Ti materials, using iron-based SMAs, which their costs are approximately 0.1 of Nitinols, can have a promising prospect in the future.

References

[1] Federal Emergency Management Agency (FEMA). State of the Art report on connection performance. Report no. FEMA 355D, Washington, D.C.; 2000.

[2] Federal Emergency Management Agency (FEMA). Recommended seismic design criteria for new moment-resisting steel frame structures. Report no. FEMA 350, Washington, D.C.; 2000.

[3] Ghobarah A, Korol RM, Osman A. Behaviour of extended end-plate connections under cyclic loading. Eng Struct 1990;12:15–27.

[4] Sumner EA, Murray TM. Behavior of extended end-plate moment connections subject to cyclic loading. J Struct Eng 2002;128(4):501–8.

[5] Tsai KC, Wu S, Popov EP. Cyclic performance of steel beam–column moment joints. Eng Struct 1995;17(8):596–602.

[6] Christopoulos C, Filiatrault A, Uang CM, Folz B. Posttensioned energy dissipating connections for moment-resisting steel frames. J Struct Eng 2002;128(9):1111–20.

[7] Ricles JM, Sause R, Peng SW, Lu LW. Experimental evaluation of earthquake resistant posttensioned steel connections. J Struct Eng 2002;128(7):850–9.

[8] Shokoohfar, M.R., Ghassemieh, M., Komeili, A. and Shakerian, M., The Influence of the Shape Memory Alloys on Concrete Shear Wall with Eccentric Openings.

[9] J. McCormick, J. Tyber, R. DesRoches, K. Gall, H. Maier, Structural engineering with NiTi Part II: mechanical behavior and scaling, J. Eng. Mech. 133 (9) (2007) 1019–1029.

[10] J. Ocel, R. DesRoches, R.T. Leon, W.G. Hess, R. Krumme, J.R. Hayes, S. Sweeney, Steel beam-column connections using shape memory alloys, J. Struct. Eng. 130 (2004) 732–740.

[11] DesRoches R, McCormick J and Delemont M 2004 Cyclic properties of superelastic shape memory alloy wires and bars J. Struct. Eng. 130 38–46

[12] DesRoches R, Taftali B and Ellingwood B R 2010 Seismic performance assessment of steel frames with shape memory alloy connections: I. Analysis and seismic demands J. Earthq. Eng. 14 471–86

[13] Ellingwood B R, Taftali B and DesRoches R 2010 Seismic performance assessment of steel frames with shape memory alloy connections: II. Probabilistic seismic demand assessment J. Earthq. Eng. 14 631–45

[14] Ma HW, Wilkinson T, Cho C. Feasibility study on a self-centering beam-to-column connection by using the superelastic behavior of SMAs. Smart Mater Struct 2007;16(5):1555–63.

[15] Ma HW, Yam MC. Experimental study on a beam-to-column connection using shape memory alloy. In: Advanced materials research, vol. 374. Trans Tech Publications; 2012. p. 2176–9

[16] Speicher MS, DesRoches R, Leon RT. Experimental results of a NiTi shape memory alloy (SMA)-based recentering beam-column connection. Eng Struct 2011;33(9):2448–57.

[17] Fang C, Yam MC, Lam AC, Xie L. Cyclic performance of extended end-plate connections equipped with shape memory alloy bolts. J Constr Steel Res 2014;94:122–36.

[18] Yam MC, Fang C, Lam AC, Zhang Y. Numerical study and practical design of beam-to-column connections with shape memory alloys. J Constr Steel Res 2015;104:177–92.

[19] Farmani MA, Ghassemieh M. Steel beam-to-column connections equipped with SMA tendons and energy dissipating devices including shear tabs or web hourglass pins. J Constr Steel Res 2017;135:30–48.

[20] Sultana P, Youssef MA. Seismic performance of steel moment resisting frames utilizing superelastic shape memory alloys. J Constr Steel Res 2016;125:239–51.

[21] Zahra Roshanfekr Rad, Mohammad Soheil Ghobadi, Mansoor Yakhchalian. Probabilistic seismic collapse and residual drift assessment of smart buildings equipped with shape memory alloy connections. Engineering Structures, vol. 197; 2019

[22] Cladera A, Weber B, Leinenbach C, Czaderski C, Shahverdi M and Motavalli M 2014 Iron-based shape memory alloys for civil engineering structures: an overview Constr. Build. Mater. 63 281–93

[23] Tanaka Y et al. 2010 Ferrous polycrystalline shape-memory alloy showing huge superelasticity Science 327 1488–90.

[24] Omori T, Ando K, Okano M, Xu X, Tanaka Y, Ohnuma I, Kainuma R and Ishida K 2011 Superelastic effect in polycrystalline ferrous alloys Science 333 68–71.

[25] Ghiami Azad, A.R., Ghassemieh, M. and Darrehzereshki, M., 2022. Numerical study of a novel bolted moment connection for beam to column connection using T-shapes and web angle sections. Sharif Journal of Civil Engineering.

[26] Fang C, Yam M C, Lam A C and Xie L 2014 Cyclic performance of extended end-plate connections equipped with shape memory alloy bolts J. Constr. Steel Res. 94 122–36.

[27] Auricchio F, Taylor R L and Lubliner J 1997 Shape-memory alloys: macromodelling and numerical simulations of the superelastic behavior Comput. Methods Appl. Mech. Eng. 146 281–312.

[28] Elsayed Mashaly, Mohamed El-Heweity, Hamdy Abou-Elfath, Mohamed Osman 2011
Behavior of four-bolt extended end-plate connection subjected to lateral loading,
Alexandria Engineering Journal.Vol. 50, Issue 1,
Pages 79-90,

[29] EN 1993-1-8:2005, Eurocode 3: design of steel structures-part 1-8: design of joints. Brussels, Belgium: European Committee for Standardization; 2005.

[30] Speicher M S, DesRoches R and Leon R T 2011 Experimental results of a NiTi shape memory alloy

(SMA)-based recentering beam-column connection Eng. Struct. 33 2448–57.

[31] SAC Joint Venture. Protocol for fabrication, inspection, testing and documentation of beam–column connection tests and other experimental specimens. Report no. SAC/BD-97/02, California; 1997.

[32] Cheng Fang, Wei Wang, Ce He, Yiyi Chen, 2017. Self-centering behavior of steel and steel-concrete composite connections equipped with NiTi SMA bolts, Engineering Structures, Vol. 150, Pages 390-408.